Synthesis and characterization of $Cs_2Pb_{1-x}Bi_xCl_2I_2$ ($0 \leq x < 0.15$) derivative perovskite

Edouard Breniaux, Edelmy J. Marin-Bernardez, Emilie Gallet, Pascal Dufour, Christophe Tenailleau *

CIRIMAT, Université de Toulouse, CNRS, Université Toulouse 3 - Paul Sabatier, 118 Route de Narbonne, 31062, Toulouse Cedex 9, France

HIGHLIGHTS

- First Bi doping of 2D RP-type $Cs_2PbCl_2I_2$ phase obtained by mechanical synthesis at RT.
- XRD data analysis and Rietveld refinements show a unit cell decrease upon Bi doping.
- A strong red-shift is observed with increasing x in $Cs_2Pb_{1-x}Bi_xCl_2I_2$ ($0 \leq x \leq 0.15$).
- Microstrains are generated in the Bi-doped $Cs_2PbCl_2I_2$ structures.

GRAPHICAL ABSTRACT

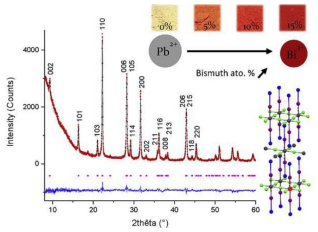

Keywords:
Halide perovskite
Mechanosynthesis
Bismuth
2D ruddlesden-popper type
Photovoltaics

ABSTRACT

Mechanosynthesis was used to obtain pure crystalline powders of a 2D Ruddlesden-Popper type $Cs_2(Pb_{1-x}Bi_x)Cl_2I_2$ phase, with $0 \leq x \leq 0.15$. These newly discovered compounds present interesting physical properties that may make them suitable for electronic devices, including LEDs and photovoltaics. Detailed structural analysis based on X-ray diffraction (XRD) data shows that lead substitution by bismuth reduces the unit cell parameters. A significant color change of the material has been observed with a clear red-shift related to the Bi doping content. The introduction of bismuth into the structure also induces strains as evidenced by XRD peak enlargements but the material can be pure up to $x = 15$ mol.%. A first ageing study shows that these strains seem to be released with time and that $Cs_2PbCl_2I_2$ and 5 mol.% Bi-doped $Cs_2PbCl_2I_2$ materials remain pure after a month in air.

1. Introduction

The world energy consumption is consistently increasing. Even though fossil resources represent most of the energy sources today, their prominent limitations make renewable systems essential for the future of humanity. Photovoltaic technology is one of them, even though it is currently limited by the efficiency, durability and cost of solar panels. In order to make solar energy more competitive and spread all over the world, optimizations need to be made in photovoltaics. This recent technology based on halide perovskites has revived the interest for photovoltaics, with 3.8% efficiency obtained in 2009 and over 25.2% PCE reached 10 years later. It represents one of the fastest increase in efficiency seen for a photovoltaic technology [1,2]. Due to these fantastic results, perovskites are becoming an important ambassador for solar energy. It is currently on the way to industrialization, as many companies are collaborating with laboratories to develop the

* Corresponding author.
E-mail address: tenailleau@chimie.ups-tlse.fr (C. Tenailleau).

https://doi.org/10.1016/j.matchemphys.2020.122870

manufacturing of stable devices. Moreover, its properties make perovskites a good candidate for a whole variety of optoelectronic devices such as photodetectors, LED, Quantum-dots for electroluminescence, lasers, or memory devices … The remaining limitation is its high sensitivity to ambient conditions, particularly to oxygen and moisture. Encapsulated systems have to be developed in order to operate solar panel for decades, in a similar way to silicon based solar cells [3].

To improve the halide perovskite stability, the decrease of its dimensionality has been proven efficient. Inserting spacers in the perovskite structure in order to disconnect blocks of octahedra in some directions (but not all) is one solution. Moisturizing effects seem then to be slowed down and the system stability improved. Usually, those spacers are organic molecules such as Butylammonium (BA) [4], Phenylethylammonium (PEA) [5] or Hexylammonium (HA) [6]. Nevertheless, organic molecules have some drawbacks, it has a low tolerance to temperature and can be harmful. The use of a totally inorganic system would avoid those main issues. Recently, Li et al. described a new "2D-type" phase, based on the so-called Ruddlesden-Popper structure. It is one of a few structures known at this day that shows a 2D halogenated all-inorganic structure. It consists of two dimensional inter-connected octahedral layers separated by either caesium or rubidium cation for all-inorganic lead or tin halide perovskites [7,8]. $Cs_2PbCl_2I_2$ exhibits a band gap close to 3 eV, not suitable for a large Sun-light energy absorption but this can be improved by substitution for solar cell applications. Besides, lead clearly needs to be replaced in halide perovskites for environmental and healthcare purposes. Bismuth can be incorporated into perovskites to replace lead. Some authors claimed for instance that it can stabilize the black alpha phase of $CsPbI_3$ for fully inorganic perovskite solar cells [9]. Heterovalent doping in lead halide perovskites is not so usual and most of halide perovskites are made in particular atmosphere conditions and/or upon heating.

Li et al. have recently described the synthesis of a new halide polycrystalline phase $Cs_2PbCl_2I_2$ by thermal treatment at 500 °C in N_2 flame-sealed tube over a period of 48 h [7]. We first managed to simplify the synthesis method by being able to obtain this phase in a conventional tube furnace at 350 °C for 12 h in air, nitrogen atmosphere being not necessary in this case (see supplementary information S1). However, attempts for doping $Cs_2PbCl_2I_2$ with bismuth in such conditions were not successful as no change on the XRD patterns were observed and traces of precursors always remained. Besides, bismuth compounds can be volatile and thermal treatments might result in a change of the expected cationic ratio.

To further simplify the synthetic procedure and in order to perform bismuth doping, we used the mechanosynthetis approach. This simple technique has also recently been used for the preparation of 3D inorganic perovskites and 2D hybrid perovskites [10–12].

This paper describes the first preparation of Bi-doped $Cs_2PbCl_2I_2$ by mechanical synthesis at room temperature without any solvent, the effects of the doping agent over the structure stability and their optical properties.

2. Materials and methods

Lead chloride powders ($PbCl_2$, 98%), caesium iodide powders (CsI, 99.9%) and bismuth chloride powders ($BiCl_3$ 98%) were purchased from Sigma-Aldrich.

Ball milling was conducted with a RETSCH PM 100 miller in an alumina bowl with 9 × 10 mm diameter alumina balls at 100 rpm up to a couple of hours. X-Ray Diffraction (XRD) measurements were conducted on a BRUKER AXS D4 Endeavor apparatus with a Copper X-ray source (wavelengths of 0.1541 nm and 0.1543 nm for K alpha 1 and 2, respectively). X-ray Fluorescence (XRF) measurements were operated on a BRUKER S2 Ranger apparatus equipped with a Palladium X-Ray source. UV–Visible absorbance was characterized with an AGILENT Uv–Vis-Nir CARY 5000 system on powders, by reflectance measurement using an integration sphere. Scanning Electron Microscopy (SEM) images were obtained on FEG JEOL JSM 7800F equipped with a Schottky type field emission.

3. Results and discussion

3.1. Synthesis and structural characterization

Halogenated precursors in stoichiometric proportions were mixed together in a mortar and grinded for 10 min before the mixture was introduced in the ball miller. After 1 h of ball milling only, pure $Cs_2PbCl_2I_2$ powder can be obtained. Up to 3 h of ball milling are necessary for forming pure $Cs_2Pb_{1-x}Bi_xCl_2I_2$ samples with the highest x values, as shown in Fig. 1a for x = 0.10 after successive milling stages, in comparison to the simulated theoretical pattern based on the literature [7]. Heterovalent doping is usually associated with concentrations of electron charges into those vacancies which are not thermodynamically favorable for the structure stability. Fig. 1b shows the XRD patterns of pure and Bi-doped $Cs_2Pb_{1-x}Bi_xCl_2I_2$ samples up to x = 0.20. The substitution limit is reached for x~0.15 as small impurity peaks corresponding essentially to CsI, PbI_2 and $PbCl_2$ are observed for x = 0.20. Further grindings did not improve the phase purity. Peak shifts are observed with a progressive increase in 2-Theta values for the (200) peak at 31.6° as x increases in $Cs_2Pb_{1-x}Bi_xCl_2I_2$ while for instance the (006) peak at 28.3° is at a similar position. Based on the ionic radii of the elements, it is assumed that Bi^{3+} ions replace Pb^{2+} ions due to steric effects ($r^{3+}_{Bi} = 1.03$ Å and $r^{2+}_{Pb} = 1.9$ Å [13]). Rietveld refinements were systematically performed on XRD data for each sample by using the FullProf Suite [14]. Background points were determined manually for each pattern. Scale factor, cell parameters, U, V and W from Caglioti's formula related to the

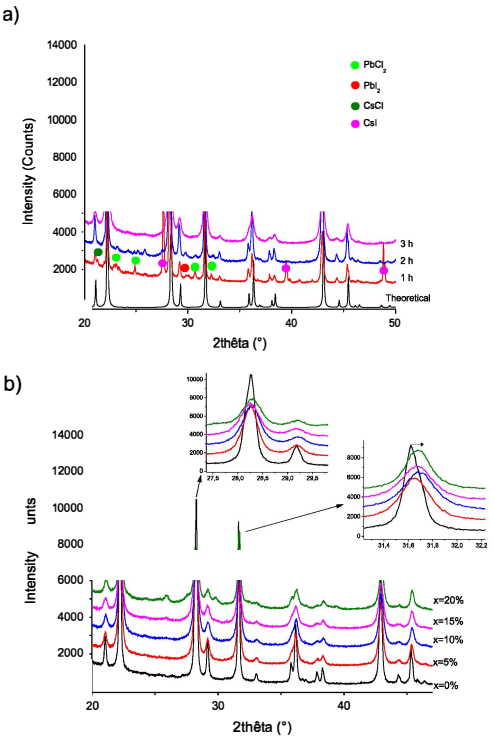

Fig. 1. a) XRD patterns of $Cs_2Pb_{0.9}Bi_{0.1}Cl_2I_2$ after different milling times b) XRD patterns of $Cs_2Pb_{1-x}Bi_xCl_2I_2$ for variable Bi contents.

Full Width at Half Maximum (FWHM), Eta and X shape parameters for the Gaussian and Lorentzian contributions in the pseudo-Voigt function, as well as the z variable atomic positions were refined for all samples. For the firstly refined pristine sample XRD pattern, zero shift, two asymmetry parameters and the overall isotropic agitation factor B, refined only for a wide scan, which was in our case for a 2Theta range varying from 8 to 100°, were also automatically adjusted by the software. The *I4/mmm* (139) space group was used with (0, 0, 0.37) atomic positions for Cs^{+}, (0.5, 0.5, 0.5) coordinates for Pb^{2+} and Bi^{3+} with the site occupancies adjusted for each element following the required proportions, (0.5, 0, 0.5) for Cl^{-} and (0.5, 0.5, 0.67) for I^{-}. For the $Cs_2PbCl_2I_2$ sample, cell parameter values obtained were $a = b = 5.6545$ (4) Å and $c = 19.005$ (2) Å, at room temperature. A zero shift value of 0.10 was found after Rietveld refinement.

When refining all the other sample data, a similar zero shift value of 0.10 ± 0.02 was given, with no particular variation as a function of the x value. This parameter was then fixed at the same value than for x = 0 before further refinement and for the final structural determination in each case. Note that when site occupancies were refined for Pb and Bi to a maximum value of 100%, the values obtained for each element was very close to the expected proportions. However, these site occupancies were fixed to the theoretical ones while refining since they are hardly distinguishable by X-rays and in order to decrease the number of refined parameters and have better accuracies on the refined values.

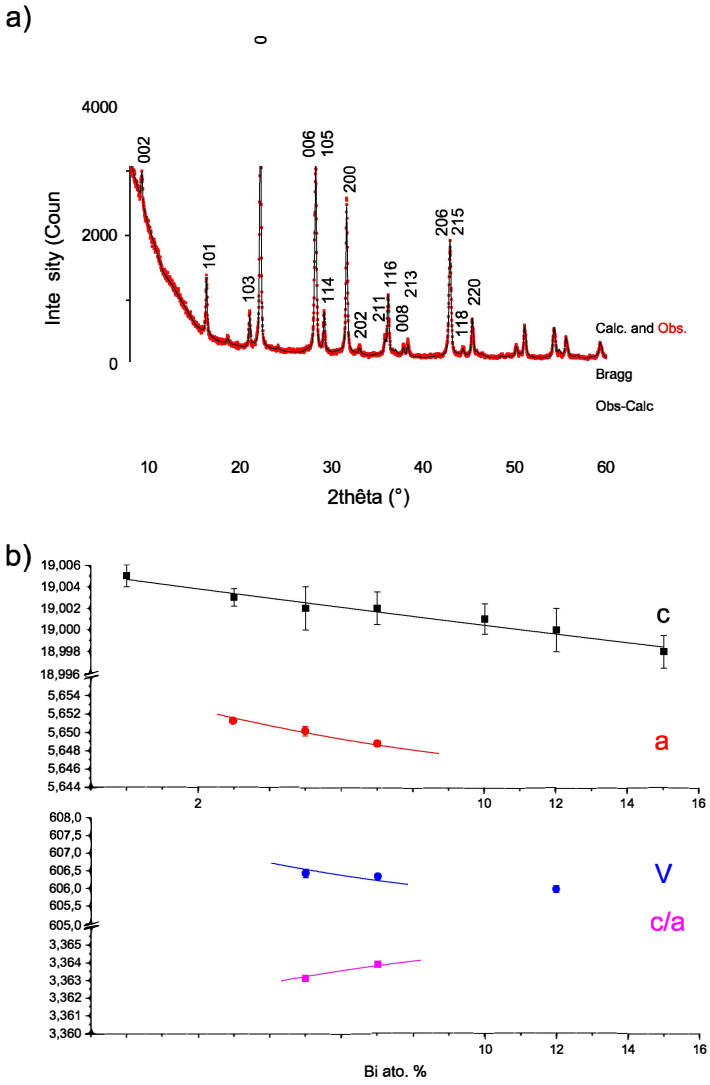

Fig. 2. a) XRD data observed (red dots) and after Rietveld refinement (black line for the calculated pattern, difference below in blue and vertical lines for Bragg peaks) for x = 3% and b) Cell parameter variations as a function of the Bi amount in $Cs_2Pb_{1-x}Bi_xCl_2I_2$. (For interpretation of the references to color in this figure legend, the reader is referred to the Web version of this article.)

Fig. 2a shows the XRD patterns as recorded and after Rietveld refinement for x = 3%. Figures of merit are always very good ($\chi^2 < 2.7$ and R_{Bragg}<0.22 from 8 to 100° in 2Theta for $0 \leq x \leq 0.15$), showing a good agreement between experimental and theoretical data. Cell parameters variations are drawn as a function of the doping agent in Fig. 2b. The unit cell volume decreases as the x value increases for $Cs_2Pb_{1-x}Bi_xCl_2I_2$, as expected since the bismuth radius is smaller than for the lead cation, though a larger cell decrease is measured in the (*a*,*b*) plane than along the *c* axis, as evidenced by the *c*/*a* ratio variation (see Fig. 2b). This results in a stronger [Pb,Bi–Cl] distance decrease in the square plane of the octahedral environment than for the [Pb,Bi–I] distance along the *c* axis.

From the XRD data analysis, we also noticed that all peaks were broader after Bi doping, especially compared to the undoped sample. This peak enlargement proportional to the Bi content increase is hard to explain although it was already reported in a recent work [15]. While it might be related to a certain degree of amorphization upon ball milling, it is actually probably due to structural deformations and in particular to the octahedral environment modifications and tilting in the perovskite derivative structure. Distorted polyhedra due to Bi-doping that exhibit a σ non-bonding pair of electrons or site disorder are common in oxide perovskites. Lone pairs can create a lattice anharmonicity. Lead halide perovskites are actually among the most anharmonic materials. But Pb^{2+} presents similar features than Bi^{3+}, so the large electrostatic repulsions created by the anion environment over the sigma orbitals should not change much from one to another if the substitution occurs at the octahedral site. Unfortunately, the free pair position is difficult to determine by X-ray diffraction due to its low density compared to the heavy atoms. FWHM broadening can be related to a change of crystallite size and/or microstrains. While crystallite sizes could not be determined after Rietveld refinement, SEM images tend to show a decrease in particle sizes upon Bi-doping and after ball milling (Fig. 3). This tendency was confirmed by particles size measurements performed on at least one hundred of particles for each image analyzed, as shown in Fig. 4. Hu et al. also observed an effect of size diminution in Bi-doped $CsPbI_3$ for nanocrystalline thin films used for solar cells [9].

The Rietveld refinement method can also give information about the microstructural characteristics of materials, based on Scherrer's formula and Williamson-Hall method. In this case, a Voigt function has to be applied by first generating a profile function that will be used as a reference for future XRD sample data refinements. The microstructural values are given for each individual reflection in order to take into account possible anisotropic effect. An apparent size close to infinity was given after Rietveld refinement meaning that no crystal size broadening could be determined.

Fig. 3. SEM images of $Cs_2Pb_{1-x}Bi_xCl_2I_2$ samples.

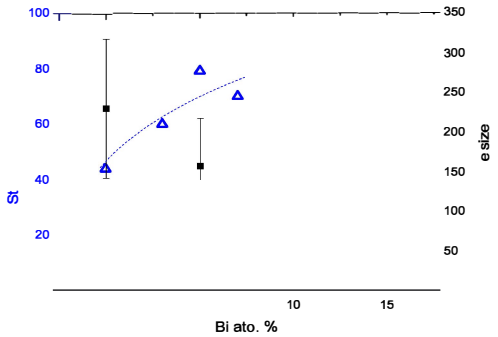

Fig. 4. Variations of microstrains and particles size as a function of bismuth doping in $Cs_2Pb_{1-x}Bi_xCl_2I_2$.

While the particle size tends to decrease upon Bi-doping, Fig. 4 shows that the maximum strains variations (in $^0/_{000}$) increases as a function of the increased Bi concentration in $Cs_2Pb_{1-x}Bi_xCl_2I_2$. These strains variation tends to saturate close to $90°/_{000}$ for the highest x values. Nayak et al. also observed a large peak broadening effect upon doping $MAPbBr_3$ with bismuth [15]. Non uniform strains or microstrains, usually induced by structural defects or reduced crystalline order, were quantified by analyzing the peak broadening in the diffraction patterns according to the modified Williamson-Hall method. The microstrains and crystal planes distortions consistently increased upon doping in their organic-inorganic 3D perovskite samples. In our work, the milling time was exactly the same for the undoped and 5% Bi-doped sample so it is hard to attribute the peak broadening in the XRD data to this effect alone. Still, microstrains increase with Bi doping while particles size decrease. This common inversed feature can be directly related to the heterovalent doping effect with the introduction of a smaller cation with a higher oxidation state (and possibly cation vacancies) into the 2D perovskite-derivative structure with a general cell decrease and a shortening of the (semi)metal-anion distances, especially in the inner planes of the octahedral layers, inducing particle size decrease and microstrains increase.

XRF measurements show that Bi is in the appropriate proportion for each sample (Fig. 5). These values were confirmed by EDS analysis (see supplementary information S2). While lead concentration decreases, the

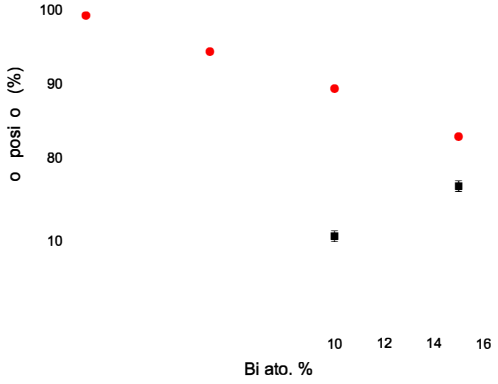

Fig. 5. *Lead (red dots) and bismuth (black squares) contents as a function of the Bi concentration as determined by XRF measurements.* (For interpretation of the references to color in this figure legend, the reader is referred to the Web version of this article.)

bismuth amount increases with the same rate. This result confirms that we successfully substituted lead by bismuth and corroborates the XRD data obtained for our synthesized samples.

3.2. Opto-electronic properties

Metal doping of materials has been widely developed in many fields in order to improve light absorption and thus efficiency of photo-electrochemical devices [9,16–20]. Fig. 6a shows the color gradient change for all our samples after synthesis. We can then assume that the redshift will probably drive to a decrease in the bandgap of the samples. Normalized absorbance spectra performed on pressed powders, after measuring the reflectance only, are shown in Fig. 6b. The absorbance is red-shifted upon Bi-doping. According to Tauc plots realized in a similar way as stipulated in literature [21], direct band gaps decrease (See supplementary information S4 for more details). But these results have to be taken with caution since the optical measurements have been performed on thick materials without considering the transmittance parameter. Bandgap narrowing was observed in other heterovalent Bi-doped halide perovskite materials, such as $CsPb_{1-x}Bi_xBr_3$ crystals and $MAPb_{1-x}Bi_xCl_3$ (MA for Methyl-Ammonium) crystals and thin films [22]. In addition, Nayak et al. showed that the band gap of few millimeters thick $MAPbBr_3$ single crystals does not change due to the presence of Bi^{3+}, despite a clear crystal color change with doping and a decrease in the absorption edge [15]. This was confirmed on thin layers of similar compositions. They stipulate that the fit of the absorbance spectra to the Elliot model does not show any significant change with the Bi content, while the band gap values decrease with Bi doping based on the Tauc plot. It is said that doping with Bi^{3+} can induce a significant increase in the sub-band gap density of states associated with the band edge tail absorption in thick samples. Besides, they found a lowering of the average photoluminescence decay in the presence of Bi which would be unfavorable to efficiency increase in solar cells. First-principles modeling of bismuth doping in $MAPbI_3$ confirmed the presence of deep trap states induced by Bi doping that facilitate transitions and can explain the absorption onset redshift observed [23].

Bismuth can also form clusters and reduce the grain size [24]. The colour change associated with Bi-doping in $MAPbBr_3$ and a bandgap narrowing was also explained by the change in density of states while introducing Bismuth "impurities", and by the stronger covalent bonding ability of Bi^{3+} which is more electronegative than Pb^{2+} and also dispose of a non-bonding pair of electrons [25]. But as it was stated recently in the literature and was mentioned above in this paper, it is most likely that Bi introduces defect states inside the bandgap [15,18]. This is the reason of a strong red-shift observed in our case (from ~2,7 to 2eV upon 15% Bi-doping), and an enhanced light absorption.

Thin film preparation of $Cs_2Pb_{1-x}Bi_xCl_2I_2$ would certainly help to verify the optical properties and check the effect of the Bi dopant over the materials band gaps. Still, the structural adjustment and increased light absorption ability of our samples remains worthy to be tested for various opto-electronic applications.

3.3. Aging – stability in ambient conditions

In order to track the stability of our samples we measured their XRD patterns up to one month after synthesis for the same amount of sample. Indeed, it is known that halide perovskites are sensitive to air and moisture. This is actually one of the main issues that needs to be solved, with lead replacement, in order to make those materials sustainable in a long term for photovoltaic systems. We noticed that the large peak widths in doped samples were systematically reduced after 7 days in air (Fig. 7). Small impurity peaks of CsI and $PbCl_2$ appeared also for the larger doping amounts tested (x = 10 and 15%), while for x = 0 and 5%, no extra peaks were observed and the phase remained pure in those latter cases (see supplementary information S3). Afterwards, no major changes in the.

XRD patterns were observed after a month of air exposure (see Fig. 7). Ball-milling performed after 7 days in air tend to broaden again the peaks for x = 5% but did not seem to affect the structures of the others, with impurities remaining for the highest x values. The micro-strains seem then to have the tendency to be released with time since the peak intensity increases while the full width at half maximum decreases for Bi-doped materials. Indeed, from Table 1 it can be seen that the increase of intensity (I) and decrease of peak broadening (H_m) for the main peak is more important for the samples containing bismuth than for the pristine sample. The rich Bi-doped materials would thus be more air sensitive. FWHM is divided by up to 2 magnitudes of order after one week of air exposure for the doped samples. The structural disorder that appears after the synthesis of Bi-doped materials seems then to rearrange after a while. Further experimental measurements such as HRTEM

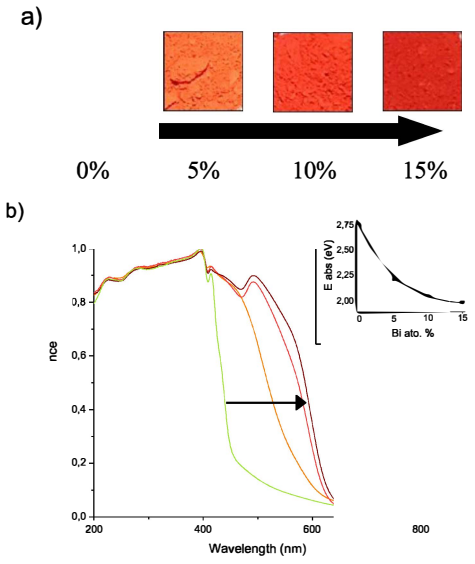

Fig. 6. a) Pictures of as-synthesized powders and b) UV Vis absorbance spectra for x = 0, 5, 10 and 15% (from left to right) determined from reflectance measurements on thick powders (without considering the transmittance contribution).

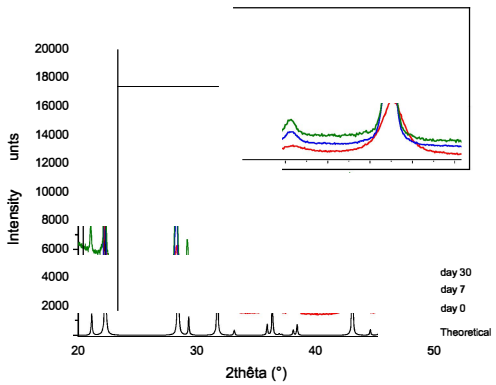

Fig. 7. Ageing study of the XRD patterns for the 10 ato. % Bi-doped $Cs_2PbCl_2I_2$ sample.

Table 1
Relative Intensity and FWHM (H_m) evolutions for the main (110) peak within a week of air exposure.

Doping (%)	I7/I0	Hm7/Hm0
0	1.18	0.71
5	2.00	0.47
10	1.89	0.47
15	1.69	0.54

need to be realized on freshly made and aged samples in order to have a better understanding of these strains and rearrangement phenomena.

4. Conclusions

We were able to obtain pure crystalline powders of 2D-type Ruddlesden-Popper inorganic halide perovskite-derivative phase of $Cs_2Pb_{1-x}Bi_xCl_2I_2$ ($0 \leq x \leq 0.15$) at room temperature within a couple of hours by mechanical synthesis. The substitution of Pb by Bi induces a cell contraction, certainly due to steric effects and to a modification of its chemical environment. Smaller particles and larger microstrains were observed upon increasing the amount of doping agent. A red-shift proportional to the bismuth content was observed on the powder samples. Structural distortion with Bi-doping and rearrangement upon air exposure were evidenced by XRD data analysis, and for $x \leq 5\%$ the materials can remain pure for at least one month.

Declaration of competing interest

The authors declare that they have no known competing financial interests or personal relationships that could have appeared to influence the work reported in this paper.

Acknowledgements

We thank Diane Samelor for her assistance in UV–Vis measurements. The International Research Experiences for Undergraduates (iREU) Program and Department of Chemistry at Xavier University of Louisiana in the USA are thanked for giving the opportunity to their student E.J. Marin-Bernardez to go to the CIRIMAT for a couple of months and gain research experience.

Appendix A. Supplementary data

Supplementary data to this article can be found online at https://doi.org/10.1016/j.matchemphys.2020.122870.

References

[1] A. Kojima, K. Teshima, Y. Shirai, T. Miyasaka, Organometal halide perovskites as visible-light sensitizers for photovoltaic cells, J. Am. Chem. Soc. 131 (2009) 6050–6051, https://doi.org/10.1021/ja809598r.
[2] Nrel Best Research-Cell Efficiency Chart, National Renewable Energy Laboratory, n.d.
[3] M. Wong-Stringer, O.S. Game, J.A. Smith, T.J. Routledge, B.A. Alqurashy, B. G. Freestone, A.J. Parnell, N. Vaenas, V. Kumar, M.O.A. Alawad, A. Iraqi, C. Rodenburg, D.G. Lidzey, High-performance multilayer encapsulation for perovskite photovoltaics, Adv. Energy Mater. 8 (2018), 1801234, https://doi.org/10.1002/aenm.201801234.
[4] J.-F. Liao, H.-S. Rao, B.-X. Chen, D.-B. Kuang, C.-Y. Su, Dimension engineering on cesium lead iodide for efficient and stable perovskite solar cells, J. Mater. Chem. A. 5 (2017) 2066–2072, https://doi.org/10.1039/C6TA09582H.
[5] J.-W. Lee, Z. Dai, T.-H. Han, C. Choi, S.-Y. Chang, S.-J. Lee, N. De Marco, H. Zhao, P. Sun, Y. Huang, Y. Yang, 2D perovskite stabilized phase-pure formamidinium perovskite solar cells, Nat. Commun. 9 (2018), https://doi.org/10.1038/s41467-018-05454-4.
[6] L. Mao, H. Tsai, W. Nie, L. Ma, J. Im, C.C. Stoumpos, C.D. Malliakas, F. Hao, M. R. Wasielewski, A.D. Mohite, M.G. Kanatzidis, Role of organic counterion in lead- and tin-based two-dimensional semiconducting iodide perovskites and application in planar solar cells, Chem. Mater. 28 (2016) 7781 7792, https://doi.org/10.1021/acs.chemmater.6b03054.
[7] J. Li, Q. Yu, Y. He, C.C. Stoumpos, G. Niu, G.G. Trimarchi, H. Guo, G. Dong, D. Wang, L. Wang, M.G. Kanatzidis, $Cs_2PbI_2Cl_2$, all-inorganic two-dimensional ruddlesden–popper mixed halide perovskite with optoelectronic response, J. Am. Chem. Soc. 140 (2018) 11085–11090, https://doi.org/10.1021/jacs.8b06046.
[8] J. Li, C.C. Stoumpos, G.G. Trimarchi, I. Chung, L. Mao, M. Chen, M.R. Wasielewski, L. Wang, M.G. Kanatzidis, Air-stable direct bandgap perovskite semiconductors: all-inorganic tin-based heteroleptic halides $A_xSnCl_yI_z$ (A = Cs, Rb), Chem. Mater. 30 (2018) 4847–4856, https://doi.org/10.1021/acs.chemmater.8b02232.
[9] Y. Hu, F. Bai, X. Liu, Q. Ji, X. Miao, T. Qiu, S. Zhang, Bismuth incorporation stabilized α-$CsPbI_3$ for fully inorganic perovskite solar cells, ACS Energy Lett 2 (2017) 2219–2227, https://doi.org/10.1021/acsenergylett.7b00508.
[10] B.A. Rosales, L. Wei, J. Vela, Synthesis and mixing of complex halide perovskites by solvent-free solid-state methods, J. Solid State Chem. 271 (2019) 206 215, https://doi.org/10.1016/j.jssc.2018.12.054.
[11] P. Pal, S. Saha, A. Banik, A. Sarkar, K. Biswas, All-Solid-state mechanochemical synthesis and post-synthetic transformation of inorganic perovskite-type halides, Chem. Eur J. 24 (2018) 1811–1815, https://doi.org/10.1002/chem.201705682.
[12] P. Sadhukhan, S. Kundu, A. Roy, A. Ray, P. Maji, H. Dutta, S.K. Pradhan, S. Das, Solvent-free solid-state synthesis of high yield mixed halide perovskites for easily tunable composition and band gap, Cryst. Growth Des. 18 (2018) 3428–3432, https://doi.org/10.1021/acs.cgd.8b00137.
[13] R.D. Shannon, Revised effective ionic radii and systematic studies of interatomic distances in halides and chalcogenides, Acta Crystallogr. A32 (1976) 751.
[14] J. Rodríguez-Carvajal, FullProf: a program for Rietveld refinement and profile matching analysis of complex powder diffraction patterns, Physica B 192 (1993) 55.
[15] P.K. Nayak, M. Sendner, B. Wenger, Z. Wang, K. Sharma, A.J. Ramadan, R. Lovrinčić, A. Pucci, P.K. Madhu, H.J. Snaith, Impact of Bi^{3+} heterovalent doping in organic–inorganic metal halide perovskite crystals, J. Am. Chem. Soc. 140 (2018) 574–577, https://doi.org/10.1021/jacs.7b11125.
[16] P.P. Patel, P.J. Hanumantha, O.I. Velikokhatnyi, M.K. Datta, D. Hong, B. Gattu, J. A. Poston, A. Manivannan, P.N. Kumta, Nitrogen and cobalt co-doped zinc oxide nanowires – viable photoanodes for hydrogen generation via photoelectrochemical water splitting, J. Power Sources 299 (2015) 11–24, https://doi.org/10.1016/j.jpowsour.2015.08.027.
[17] X. Yang, A. Wolcott, G. Wang, A. Sobo, R.C. Fitzmorris, F. Qian, J.Z. Zhang, Y. Li, Nitrogen-doped ZnO nanowire arrays for photoelectrochemical water splitting, Nano Lett. 9 (2009) 2331–2336, https://doi.org/10.1021/nl900772q.
[18] P.P. Patel, P.J. Hanumantha, O.I. Velikokhatnyi, M.K. Datta, B. Gattu, J.A. Poston, A. Manivannan, P.N. Kumta, Vertically aligned nitrogen doped (Sn,Nb)O2 nanotubes – robust photoanodes for hydrogen generation by photoelectrochemical water splitting, Mater. Sci. Eng. B 208 (2016) 1–14, https://doi.org/10.1016/j.mseb.2016.02.001.
[19] A.K. Jena, A. Kulkarni, Y. Sanehira, M. Ikegami, T. Miyasaka, Stabilization of α-$CsPbI_3$ in ambient room temperature conditions by incorporating Eu into $CsPbI_3$, Chem. Mater. 30 (2018) 6668–6674, https://doi.org/10.1021/acs.chemmater.8b01808.
[20] M. Wang, K. Deng, L. Meng, L. Li, Bifunctional ytterbium (III) chloride driven low-temperature synthesis of stable α-$CsPbI_3$ for high-efficiency inorganic perovskite solar cells, Small Methods (2019) 1900652, https://doi.org/10.1002/smtd.201900652.
[21] T. Ruf, S. Repp, J. Urban, R. Thomann, E. Erdem, Competing effects between intrinsic and extrinsic defects in pure and Mn-doped ZnO nanocrystals, J. Nanoparticle Res. 18 (2016), https://doi.org/10.1007/s11051-016-3408-z.
[22] Z. Zhang, L. Ren, H. Yan, S. Guo, S. Wang, M. Wang, K. Jin, Bandgap narrowing in Bi-doped $CH_3NH_3PbCl_3$ perovskite single crystals and thin films, J. Phys. Chem. C 121 (2017) 17436–17441, https://doi.org/10.1021/acs.jpcc.7b06248.
[23] E. Mosconi, B. Merabet, D. Meggiolaro, A. Zaoui, F. De Angelis, First-principles modeling of bismuth doping in the $MAPbI_3$ perovskite, J. Phys. Chem. C 122 (2018) 14107–14112, https://doi.org/10.1021/acs.jpcc.8b01307.
[24] H.-T. Sun, J. Zhou, J. Qiu, Recent advances in bismuth activated photonic materials, Prog. Mater. Sci. 64 (2014) 1–72, https://doi.org/10.1016/j.pmatsci.2014.02.002.
[25] A.L. Abdelhady, M.I. Saidaminov, B. Murali, V. Adinolfi, O. Voznyy, K. Katsiev, E. Alarousu, R. Comin, I. Dursun, L. Sinatra, E.H. Sargent, O.F. Mohammed, O. M. Bakr, Heterovalent dopant incorporation for bandgap and type engineering of perovskite crystals, J. Phys. Chem. Lett. 7 (2016) 295 301, https://doi.org/10.1021/acs.jpclett.5b02681.